








RESEARCH ARTICLE | AUGUST 22 2022

Inertially amplified seismic metamaterial with an ultra-low-frequency bandgap

Special Collection: [Acoustic and Elastic Metamaterials and Metasurfaces](#)Yi Zeng ; Liyun Cao; Sheng Wan; Tong Guo; Shuowei An; Yan-Feng Wang ; Qiu-Jiao Du ; Brice Vincent; Yue-Sheng Wang  ; Badreddine Assouar  *Appl. Phys. Lett.* 121, 081701 (2022)<https://doi.org/10.1063/5.0102821>

Articles You May Be Interested In

A snowman-like seismic metamaterial

J. Appl. Phys. (September 2022)

Low-frequency broadband seismic metamaterial using I-shaped pillars in a half-space

J. Appl. Phys. (May 2018)

A special eigenmode to induce bandgap and attenuate low-frequency seismic surface waves

AIP Advances (October 2024)

Applied Physics Letters

Special Topics Open for Submissions

[Learn More](#)

Inertially amplified seismic metamaterial with an ultra-low-frequency bandgap

Cite as: Appl. Phys. Lett. **121**, 081701 (2022); doi: [10.1063/5.0102821](https://doi.org/10.1063/5.0102821)

Submitted: 13 June 2022 · Accepted: 3 August 2022 ·

Published Online: 22 August 2022



View Online



Export Citation



CrossMark

Yi Zeng,^{1,2} Liyun Cao,¹ Sheng Wan,¹ Tong Guo,¹ Shuwei An,³ Yan-Feng Wang,² Qiu-Jiao Du,⁴ Brice Vincent,¹ Yue-Sheng Wang,^{2,5,a)} and Badreddine Assouar^{1,a)}

AFFILIATIONS

¹Université de Lorraine, CNRS, Institut Jean Lamour, Nancy 54000, France

²Department of Mechanics, School of Mechanical Engineering, Tianjin University, Tianjin 300350, China

³Department of Mechanical Engineering, The Hong Kong Polytechnic University, Hung Hom, Kowloon, Hong Kong SAR, China

⁴School of Mathematics and Physics, China University of Geosciences, Wuhan 430074, China

⁵Department of Mechanics, Beijing Jiaotong University, Beijing 100044, China

Note: This paper is part of the APL Special Collection on Acoustic and Elastic Metamaterials and Metasurfaces.

a) Authors to whom correspondence should be addressed: yswang@tju.edu.cn and badreddine.assouar@univ-lorraine.fr

ABSTRACT

In last two decades, it has been theoretically and experimentally demonstrated that seismic metamaterials are capable of isolating seismic surface waves. Inertial amplification mechanisms with small mass have been proposed to design metamaterials to isolate elastic waves in rods, beams, and plates at low frequencies. In this Letter, we propose an alternative type of seismic metamaterial providing an ultra-low-frequency bandgap induced by inertial amplification. A unique kind of inertially amplified metamaterial is first conceived and designed. Its bandgap characteristics for flexural waves are then numerically and experimentally demonstrated. Finally, the embedded inertial amplification mechanism is introduced on a soil substrate to design a seismic metamaterial capable of strongly attenuating seismic surface waves around a frequency of 4 Hz. This work provides a promising alternative way to conceive seismic metamaterials to steer and control surface waves.

Published under an exclusive license by AIP Publishing. <https://doi.org/10.1063/5.0102821>

Seismic metamaterials (SMs), used to control seismic surface waves at low frequencies, have been investigated and proposed to protect critical infrastructures and ancient buildings in the last two decades.^{1–7} The SMs composed of an array of artificial structures on or in a soil substrate usually possess the bandgap characteristics, whose working wavelengths are much longer than the size of the artificial structure.^{4–10} A number of experiments^{1,3,11} and simulations^{5,12–14} have demonstrated that the SMs can significantly attenuate seismic waves at the frequencies of the bandgaps. In 1999, a phononic crystal in a marble was designed to experimentally demonstrate the existence of elastic bandgaps and the possible applications of SMs.¹ Farhat *et al.*¹⁵ proposed a design for a radially symmetric multilayered cloak to control flexural waves propagating in isotropic heterogeneous thin plates. The large-scale experiments, proposed by Brûlé *et al.*,³ have demonstrated that the SMs constituted of cylindrical holes periodically arranged in a soil substrate can attenuate seismic surface waves around a frequency of 50 Hz. It is easy to find evidence that the working frequency is not low enough to protect and shield human buildings. As Kadic *et al.*¹⁶ commented, the large-scale experiments are still far from being a

functional cloak. Therefore, the SMs based on local resonance^{17–20} were proposed to obtain low-frequencies bandgaps for seismic surface waves. Finocchio *et al.*²¹ introduced the mass-in-mass system in the soil to filter the harmonics of seismic waves at the fundamental resonance frequency of the building. Also, researchers proposed SMs composed of an array of pillars on a soil substrate to achieve low-frequencies bandgap, when they got inspiration that the seismic waves can be attenuated by the forests.^{5,9,22} To obtain wide bandgaps, different kinds of shape of the pillars^{6,11,23,24} were proposed, and the “rainbow trapping effects”^{9,14,25–27} were used. However, at present, the bandgap for seismic surface waves below 5 Hz is still challenging to obtain just by using small-mass structures.

An inertial amplification mechanism,^{28,29} which can achieve low-frequency resonance just by using small mass, has been introduced to design elastic metamaterials to obtain low-frequencies bandgaps. In 2006, Yilmaz and Kikuchi³⁰ designed a passive low-pass filter-type vibration with low stop band frequencies by using the lever-type structures. Then, the hybrid lever-type isolation systems with X-shaped structures were proposed to improve the band-stop characteristics at

low frequencies.^{31,32} In addition, the embedded amplification mechanism was proposed by Yilmaz *et al.*^{28,29} to amplify the effective inertia of the wave propagation medium. Frandsen *et al.*³³ introduced the similar structures into a continuous elastic rod to obtain wide bandgap induced by inertial amplification. The three-dimensional metamaterials based on an embedded inertial amplification mechanism have been realized. It has been experimentally demonstrated that they are capable of isolating elastic waves in a wide frequency range.³⁴ Then, Yuksel and Yilmaz³⁵ have designed a two-dimensional solid structure with embedded inertial amplification mechanisms by using topology optimization to achieve an ultra-wide stop band at low frequencies. However, the embedded inertial amplification mechanisms have not been introduced into a half space to isolate surface waves.

In this Letter, we propose a unique kind of SM with an ultra-low-frequency bandgap for seismic surface waves by using embedded inertial amplification mechanisms. At first, we design a kind of one-dimensional inertially amplified metamaterial (IAM). The unit cell of the IAM is composed of one base beam, two arms, and three hinge joints. The characteristics of the bandgap induced by inertial amplification in the IAM are investigated by using experiments and simulations. Finally, the embedded inertial amplification mechanism is introduced to design the SMs for surface waves at ultra-low frequencies.

Three different samples are illustrated in Fig. 1(a). The geometric parameter of the bare beam (BB) is $180 \times 30 \times 1 \text{ mm}^3$. The traditional metamaterial (TM) has three more rectangles than the bare beam. The geometric parameter of the rectangle is $49 \times 9.8 \times 6 \text{ mm}^3$.

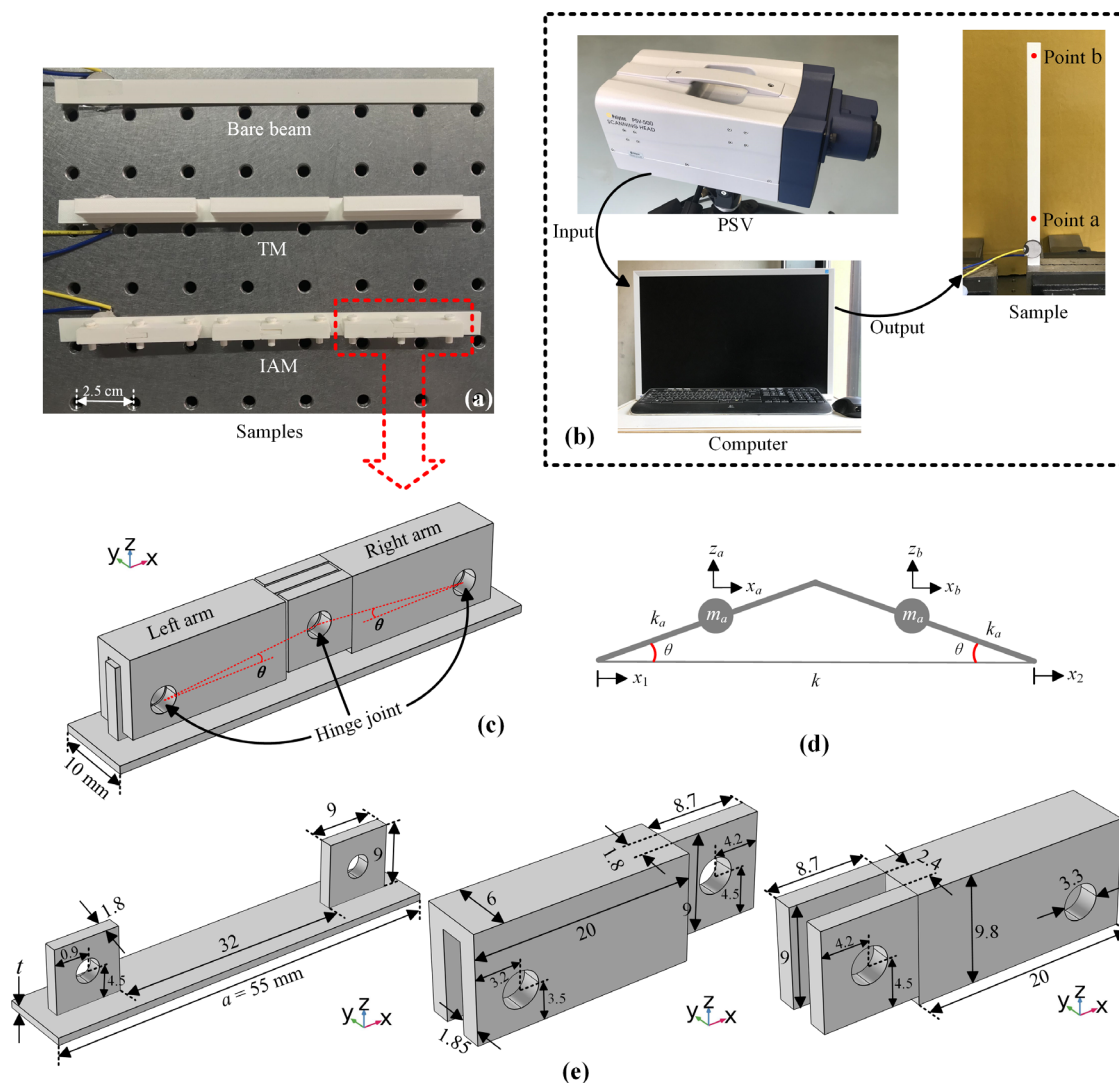


FIG. 1. (a) The samples used in the experiments (TM: traditional metamaterial; IAM: inertially amplified metamaterial). (b) Schematic diagram of the experimental setup, including the laser vibrometer (PSV), the computer, and the sample. Points a and b are two data collection points. (c) The unit cell of the IAM. (d) The simplified model of the inertially amplified mechanism in the unit cell and (e) the geometric parameters of the unit cell of the IAM.

The inertially amplified metamaterial (IAM) has three more inertial amplification mechanisms than the bare beam. The lattice constant of the TM and IAM is all 55 mm. All the samples are fabricated by the 3D printer based on polylactic acid (PLA). The material parameters of PLA are shown in Table I.^{36,37} Figure 1(b) illustrates the schematic diagram of the experimental setup. The computer outputs the source signal to the piezoelectric patches fixed at the end of the sample. The out-of-plane accelerations at points a and b are measured by the laser vibrometer (Polytec PSV-500). The collected data are input back to the computer and are processed. It is noted that the position of points a and b is all at the back of the samples.³⁷

Figure 1(c) illustrates the unit cell of the IAM considered in numerical simulations and experiments. The unit cell includes one base beam, two arms, and three hinge joints. The thickness t of the beam is 1 mm. The angle θ , which determines the magnitude of the amplification generated by the inertially amplified mechanisms, in this work is set at 5° . It is worth noting that the hinge joint is not the necessary part for inertial amplification mechanisms. As shown in the literature, Yilmaz and Kikuchi³⁰ designed a passive low-pass filter-type vibration with low stop band frequencies by using the lever-type structures without hinge joint. However, the hinge joint is a simple way to achieve the inertial amplification mechanism in the metamaterials. Such as in other works, Frandsen *et al.*³³ introduced the inertial amplification mechanism into a continuous elastic rod to obtain wide bandgap by using the hinge joints.

The simplified model of the inertially amplified mechanism of the unit cell of the IAM is illustrated in Fig. 1(d). The m_a takes the value of the mass of one arm in the middle of the arm. The k and k_a mean the stiffness of the beam and arm, respectively. Here, the k_a can be regarded as rigid at ultra-low frequencies. The angle θ between the arm and the beam is 5° . All the geometric parameters are shown in Figs. 1(c) and 1(e). It is noted that the lattice constant a is 55 mm, and the unit of all the geometric parameters is millimeter.

In Fig. 1(d), the x_1 and x_2 represent the displacement of the input and output, respectively. At ultra-low frequencies, the horizontal and vertical displacement of the two m_a are

$$x_a = \frac{(3x_1 + x_2)}{4}, \quad (1)$$

$$z_a = \cot(\theta) \frac{(x_1 - x_2)}{4}, \quad (2)$$

$$x_b = \frac{(x_1 + 3x_2)}{4}, \quad (3)$$

$$z_b = \cot(\theta) \frac{(x_1 - x_2)}{4}. \quad (4)$$

Therefore, the kinetic energy (T) and potential energy (V) of the system are

TABLE I. The material parameters used in this Letter.

Material	Density (kg/m ³)	Young's modulus (Pa)	Poisson's ratio
PLA	1086.3	3.4398×10^9	0.35
Steel	7784	2.07×10^{11}	0.3
Soil	1800	2×10^7	0.3

$$T = \frac{m_a(\dot{x}_a^2 + \dot{z}_a^2)}{2} + \frac{m_a(\dot{x}_b^2 + \dot{z}_b^2)}{2}, \quad (5)$$

$$V = \frac{k(x_2 - x_1)^2}{2}. \quad (6)$$

From Lagrange's equation, i.e.,

$$0 = \frac{d}{dt} \left(\frac{\partial L}{\partial \dot{x}_2} \right) - \frac{\partial L}{\partial x_2}, \quad (7)$$

where L is the Lagrange function

$$L = T - V. \quad (8)$$

Substituting Eq. (8) into Eq. (7), we obtain

$$\left(\frac{2m_a[5 + \cot^2(\theta)]}{16} \right) \ddot{x}_2 + kx_2 = \frac{2m_a[\cot^2(\theta) - 2]}{16} \ddot{x}_1 + kx_1. \quad (9)$$

When the two sides of Eq. (9) are equal to zero, the first resonance (ω_r) and first anti-resonance (ω_{ar})^{33,35,38} frequencies are obtained

$$\omega_r = \sqrt{\frac{k}{2m_a[5 + \cot^2(\theta)]/16}}, \quad (10)$$

$$\omega_{ar} = \sqrt{\frac{k}{2m_a[\cot^2(\theta) - 2]/16}}. \quad (11)$$

As can be seen from Eqs. (10) and (11), the ω_r is always lower than the ω_{ar} . When the angle θ is less than 16.7° , the function $\eta = [5 + \cot^2(\theta)]/16$ is larger than 1, which means the amplified motion for the mass is caused by the inertially amplified mechanism, and the inertial mass is amplified η times. Of course, according to Eq. (10), if the stiffness k is weaker or the mass of two arms is heavier, the lower ω_r can be obtained. It is worth noting that, comparing with the metamaterials based on local resonance,^{39,40} the inertial amplification mechanism is also based on the local resonance, which can be found from Eq. (10), but it can easily obtain lower-frequency bandgap because of the function $\eta = [5 + \cot^2(\theta)]/16$ appeared in Eq. (10). For example, in this work, the angle θ is 5° , so the inertial mass is amplified about 8.5 times. Therefore, the small mass can achieve strong resonance at low frequencies.

In the simulations, all results are calculated by using finite element software COMSOL 5.4 (Multibody Dynamics Module). The Floquet–Bloch boundary conditions are achieved on the unit cell along the x direction by using both boundary similarity and pointwise constraint. In Fig. 1(e), the hinge-connection condition is set on the hinge joints between two bodies. The transmission spectra of the flexural waves in experiments and simulations are defined as

$$TS = 20 \times \log_{10}(R_b/R_a), \quad (12)$$

where R_a and R_b are the root mean square (RMS) of the out-of-plane velocities at points a and b shown in Fig. 1(b), respectively.

Figure 2(a) illustrates the band structure of the IAM along the x direction, and the color bar represents the degree of the out-of-plane polarization. The parameter ξ is used to define the degree of the out-of-plane polarization

$$\xi = \left| \int_C w dC \right| / \left| \int_C |disp| dC \right|, \quad (13)$$

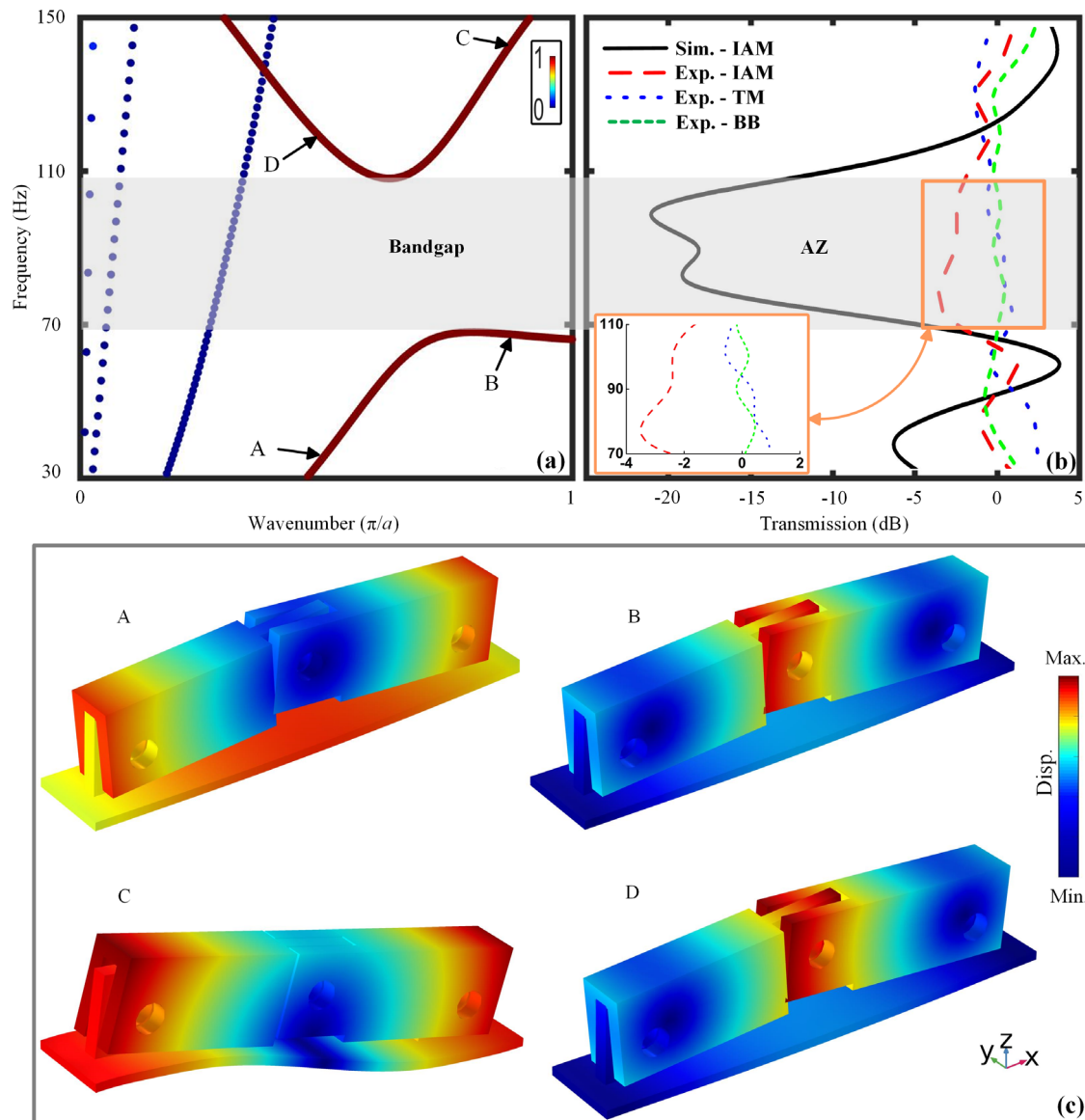


FIG. 2. (a) The band structure of the IAM. The color bar represents the degree of the out-of-plane polarization. (b) The transmission spectra of the flexural waves in the IAM, the TM, and the BB (bare beam). The AZ is the attenuation zone. (c) Vibration modes corresponding to points A–D shown in (a). The color bar in (c) represents the degree of displacement.

where w is the integral of the z component of the displacement fields in the yz -cut plane (to avoid the effect of the torsional modes in the beam), $disp.$ is the total displacement, and C means the whole unit cell. Therefore, in Fig. 2(a), it is obvious that a bandgap induced by inertial amplification is generated for flexural waves in the frequency range from 70 to 108 Hz.

As shown in Fig. 2(b), in the frequency range of the bandgap, a significant attenuation zone (AZ) can be found in the simulation results. Comparing with all the experimental results, the IAM has an attenuation zone for the flexural waves around from 70 to 108 Hz. Indeed, the experimentally measured attenuation of the IAM is far

inferior compared to the simulated one. This is due to the fact that the hinge joints are rigid and smooth in the simulations but not in the experiments. However, comparing with other two experimental samples (bare beam and TM), the attenuation zone is not difficult to find. It is noted the unit cell of the TM has more mass than the IAM, but the frequency of the first bandgap of the TM for flexural waves is much higher than the IAM. The band structure of the TM, which is easy to calculate just by using the solid module of the COMSOL,^{3,4,11,41} is not illustrated in this Letter.

Figure 2(c) illustrates the vibration modes at marked points A–D in the band structure shown in Fig. 2(a). At points A and C, the

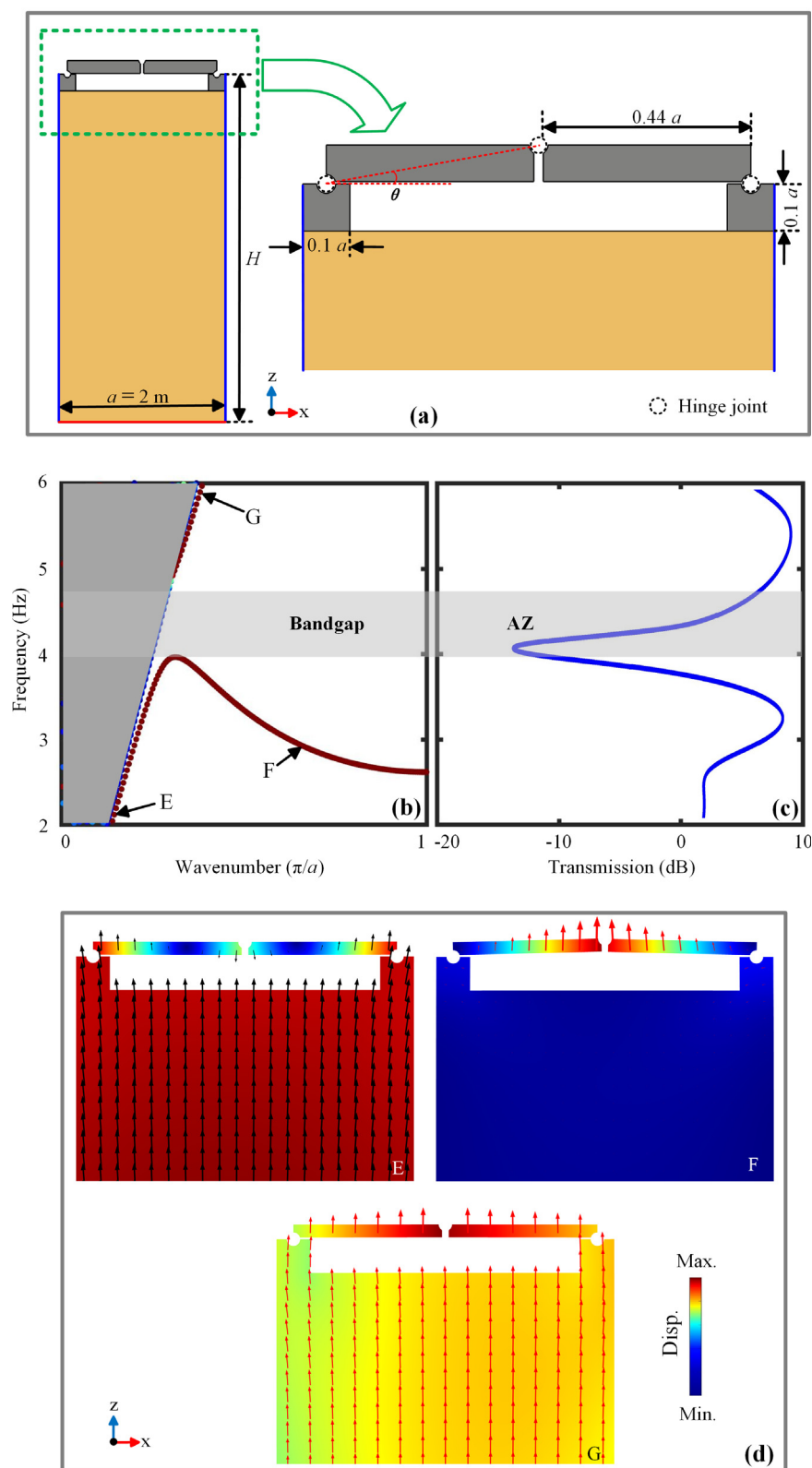


FIG. 3. (a) The unit cell of the SM with an embedded inertial amplification mechanism. The blue and red lines represent Floquet–Bloch boundary conditions and fixed constraint, respectively. The dotted circle represents the hinge joint between two bodies. (b) The band structure of the SM. (c) The transmission spectrum of the surface waves in the SM with seven unit cells. (d) Vibration modes corresponding to points E–G shown in (b). The color bar in (d) represents the degree of displacement. The arrows indicate the displacement eigenvector, whose length and direction represent the magnitude and trend of the particle movement, respectively.

significant displacement appears in the beam and around the hinge joints between beam and arms. Due to the similar vibration modes and slopes (in the band structure) of these two points, it is clear that these two points come from the same band, which is opened by the bandgap. This is common in the band structures of the metamaterials based on local resonance.^{42–44} At points B and D, almost all the displacement appears around the hinge joint between two arms, which means that there is a strong resonance only on the two arms. Based on this information, it is not difficult to infer that the low-frequencies bandgap is opened by the local resonance of the inertial amplification mechanism.

It is noted that the simplified model of the embedded inertial amplification mechanism shown in Fig. 1(d) can also theoretically work on a half-space when the substrate provides the stiffness k . Therefore, in theory, the embedded inertial amplification mechanism is very suitable to design surface wave metamaterials, which, just with small mass, can induce low-frequency bandgap for surface waves. As shown in Fig. 3(a), the embedded inertial amplification mechanism is introduced on a half-space to attenuate seismic surface waves. The unit cell of the seismic metamaterial (SM) is constituted of three parts: two steel arms represented by gray area, three hinge joints represented by dotted circle, and the soil substrate represented by yellow area. The blue and red lines represent the Floquet–Bloch boundary condition and fixed constraint, respectively. The lattice constant a in Fig. 3(a) is 2 m, and the depth of the soil substrate is $H = 500a$.^{11,37} The angle θ is also 5° , and other geometric parameters are shown in Fig. 3(a). The material parameters of the steel and soil used in this Letter are shown in Table I.

Figure 3(b) illustrates the band structure of the one-dimension periodic SM. The sound cone and the bandgap for surface waves are represented by the dark gray and light gray zones, respectively. The bandgap is in the range from 4.0 to 4.7 Hz, and the relative bandwidth is 0.16. Despite the narrow width of this bandgap, the definitive existence of this bandgap is encouraging. It is noted that the SM based on the embedded inertial amplification mechanism with smaller mass can achieve a bandgap with larger relative bandwidth than the SM based on the inertial amplification mechanism³⁷ at low frequencies. As shown in Fig. 3(c), it is the transmission spectrum of the surface waves in the SM with seven unit cells.^{11,45,46} An attenuation peak can be found around at 4 Hz. The band structure of the SM and the attenuation effects of the surface waves in the SM all demonstrate that the existence of the ultra-low-frequencies bandgap.

Figure 3(d) illustrates the vibration modes at marked points E–G in the band structure shown in Fig. 3(b). The arrows shown in the unit cell indicate the displacement eigenvector, whose length and direction represent the magnitude and trend of the particle movement, respectively. At points E and G, the significant displacement appears both in the soil substrate and the arms. At point F, almost all the displacement appears around the hinge joint between the two arms, which is similar to the bandgap shown in Fig. 2. The strong local resonance appears only on the two arms of the inertial amplification mechanism. It demonstrates the bandgap for surface waves is induced by the inertial amplification.

In summary, an alternative type of seismic metamaterial with an ultra-low-frequency bandgap induced by inertial amplification has been presented and discussed to isolate seismic surface waves. We first have proposed a one-dimensional inertially amplified metamaterial,

whose unit cell is composed of one base beam, two arms, and three hinge joints. The experimental and simulated results of transmissions of the flexural waves in the bare beam, traditional metamaterial, and inertially amplified metamaterial have demonstrated that the inertially amplified metamaterial is capable of isolating flexural waves in the bandgap induced by inertial amplification. Finally, the embedded inertial amplification mechanism has been introduced on a soil half-space to design the seismic metamaterial. The band structure and the transmission results have shown that the seismic metamaterial can isolate seismic Rayleigh waves at ultra-low frequencies. It is worth noting that the embedded inertial amplification mechanisms with small mass can strongly attenuate elastic waves at ultra-low frequencies, which is a very needed and sought property for seismic metamaterials. This work indicates that the embedded inertial amplification mechanisms can induce bandgaps for seismic surface waves at ultra-low frequencies.

This work was supported by la Région Grand Est, the Institut CARNOT ICEEL, and the National Natural Science Foundation of China (Grant Nos. 12021002, 12122207, 11991031, 11991032, and 41974059). The first author is grateful to the support of the China Scholarship Council (Grant No. 202006250084).

AUTHOR DECLARATIONS

Conflict of Interest

The authors have no conflicts to disclose.

Author Contributions

Yi Zeng: Conceptualization (equal); Data curation (equal); Formal analysis (equal); Investigation (equal); Methodology (equal); Validation (equal); Writing – original draft (equal); Writing – review and editing (equal). **Badreddine Assouar:** Conceptualization (equal); Formal analysis (equal); Funding acquisition (equal); Supervision (equal); Validation (equal); Writing – original draft (equal); Writing – review and editing (equal). **Liyun Cao:** Data curation (equal); Formal analysis (equal); Investigation (equal). **Sheng Wan:** Data curation (equal); Formal analysis (equal); Investigation (equal). **Tong GUO:** Data curation (equal); Formal analysis (equal). **Shuo-wei An:** Data curation (equal); Formal analysis (equal). **Yan-Feng Wang:** Data curation (equal); Formal analysis (equal); Investigation (equal). **Qiujiao Du:** Data curation (equal); Formal analysis (equal); Investigation (equal). **Brice Vincent:** Data curation (equal); Investigation (equal). **Yue-Sheng Wang:** Conceptualization (equal); Formal analysis (equal); Funding acquisition (equal); Supervision (equal); Validation (equal); Writing – original draft (equal); Writing – review and editing (equal).

DATA AVAILABILITY

The data that support the findings of this study are available from the corresponding authors upon reasonable request.

REFERENCES

- ¹F. Meseguer, M. Hologado, D. Caballero, N. Benaches, J. Sánchez-Dehesa, C. López, and J. Llinares, “Rayleigh-wave attenuation by a semi-infinite two-dimensional elastic-band-gap crystal,” *Phys. Rev. B* **59**, 12169 (1999).
- ²S.-H. Kim and M. P. Das, “Artificial seismic shadow zone by acoustic metamaterials,” *Mod. Phys. Lett. B* **27**, 1350140 (2013).

- ³S. Brülé, E. Javelaud, S. Enoch, and S. Guenneau, "Experiments on seismic metamaterials: Molding surface waves," *Phys. Rev. Lett.* **112**, 133901 (2014).
- ⁴M. Miniaci, A. Krushynska, F. Bosia, and N. M. Pugno, "Large scale mechanical metamaterials as seismic shields," *New J. Phys.* **18**, 083041 (2016).
- ⁵A. Colombi, P. Roux, S. Guenneau, P. Gueguen, and R. V. Craster, "Forests as a natural seismic metamaterial: Rayleigh wave bandgaps induced by local resonances," *Sci. Rep.* **6**, 19238 (2016).
- ⁶Y. Zeng, Y. Xu, K. Deng, Z. Zeng, H. Yang, M. Muzamil, and Q. Du, "Low-frequency broadband seismic metamaterial using I-shaped pillars in a half-space," *J. Appl. Phys.* **123**, 214901 (2018).
- ⁷X. Wang, S. Wan, Y. Nian, P. Zhou, and Y. Zhu, "Periodic in-filled pipes embedded in semi-infinite space as seismic metamaterials for filtering ultra-low-frequency surface waves," *Constr. Build. Mater.* **313**, 125498 (2021).
- ⁸N. Aravantinos-Zafiris and M. Sigalas, "Large scale phononic metamaterials for seismic isolation," *J. Appl. Phys.* **118**, 064901 (2015).
- ⁹A. Colombi, D. Colquitt, P. Roux, S. Guenneau, and R. V. Craster, "A seismic metamaterial: The resonant metawedge," *Sci. Rep.* **6**, 27717 (2016).
- ¹⁰Y. Achaoui, T. Antonakakis, S. Brülé, R. V. Craster, S. Enoch, and S. Guenneau, "Clamped seismic metamaterials: Ultra-low frequency stop bands," *New J. Phys.* **19**, 063022 (2017).
- ¹¹Y. Zeng, S.-Y. Zhang, H.-T. Zhou, Y.-F. Wang, L. Cao, Y. Zhu, Q.-J. Du, B. Assouar, and Y.-S. Wang, "Broadband inverted T-shaped seismic metamaterial," *Mater. Des.* **208**, 109906 (2021).
- ¹²Q. Du, Y. Zeng, G. Huang, and H. Yang, "Elastic metamaterial-based seismic shield for both Lamb and surface waves," *AIP Adv.* **7**, 075015 (2017).
- ¹³Y. Chen, Q. Feng, F. Scarpa, L. Zuo, and X. Zhuang, "Harnessing multi-layered soil to design seismic metamaterials with ultralow frequency band gaps," *Mater. Des.* **175**, 107813 (2019).
- ¹⁴W. Liu, G. H. Yoon, B. Yi, Y. Yang, and Y. Chen, "Ultra-wide band gap metasurfaces for controlling seismic surface waves," *Extreme Mech. Lett.* **41**, 101018 (2020).
- ¹⁵M. Farhat, S. Guenneau, and S. Enoch, "Ultrabroadband elastic cloaking in thin plates," *Phys. Rev. Lett.* **103**, 024301 (2009).
- ¹⁶M. Kadic, T. Bückmann, R. Schittny, and M. Wegener, "Metamaterials beyond electromagnetism," *Rep. Prog. Phys.* **76**, 126501 (2013).
- ¹⁷Z. Liu, X. Zhang, Y. Mao, Y. Zhu, Z. Yang, C. Chan, and P. Sheng, "Locally resonant sonic materials," *Science* **289**, 1734–1736 (2000).
- ¹⁸P. Sheng, X. X. Zhang, Z. Liu, and C. T. Chan, "Locally resonant sonic materials," *Physica B* **338**, 201–205 (2003).
- ¹⁹Y. Zeng, Y. Xu, K. Deng, P. Peng, H. Yang, M. Muzamil, and Q. Du, "A broadband seismic metamaterial plate with simple structure and easy realization," *J. Appl. Phys.* **125**, 224901 (2019).
- ²⁰Y. Zeng, P. Peng, Q.-J. Du, Y.-S. Wang, and B. Assouar, "Subwavelength seismic metamaterial with an ultra-low frequency bandgap," *J. Appl. Phys.* **128**, 014901 (2020).
- ²¹G. Finocchio, O. Casablanca, G. Ricciardi, U. Alibrandi, F. Garesci, M. Chiappini, and B. Azzerboni, "Seismic metamaterials based on isochronous mechanical oscillators," *Appl. Phys. Lett.* **104**, 191903 (2014).
- ²²Y.-F. Liu, J.-K. Huang, Y.-G. Li, and Z.-F. Shi, "Trees as large-scale natural metamaterials for low-frequency vibration reduction," *Constr. Build. Mater.* **199**, 737–745 (2019).
- ²³Muhammad, C. Lim and J. Reddy, "Built-up structural steel sections as seismic metamaterials for surface wave attenuation with low frequency wide bandgap in layered soil medium," *Eng. Struct.* **188**, 440–451 (2019).
- ²⁴Y. Zeng, Y. Xu, H. Yang, M. Muzamil, R. Xu, K. Deng, P. Peng, and Q. Du, "A Matryoshka-like seismic metamaterial with wide band-gap characteristics," *Int. J. Solids Struct.* **185–186**, 334–341 (2020).
- ²⁵X. Pu, A. Palermo, Z. Cheng, Z. Shi, and A. Marzani, "Seismic metasurfaces on porous layered media: Surface resonators and fluid-solid interaction effects on the propagation of Rayleigh waves," *Int. J. Eng. Sci.* **154**, 103347 (2020).
- ²⁶S. Krödel, N. Thomé, and C. Daraio, "Wide band-gap seismic metastructures," *Extreme Mech. Lett.* **4**, 111–117 (2015).
- ²⁷Y. Zeng, L. Cao, Y. Zhu, Y.-F. Wang, Q.-J. Du, Y.-S. Wang, and B. Assouar, "Coupling the first and second attenuation zones in seismic metasurface," *Appl. Phys. Lett.* **119**, 013501 (2021).
- ²⁸C. Yilmaz, G. M. Hulbert, and N. Kikuchi, "Phononic band gaps induced by inertial amplification in periodic media," *Phys. Rev. B* **76**, 054309 (2007).
- ²⁹C. Yilmaz and G. Hulbert, "Theory of phononic gaps induced by inertial amplification in finite structures," *Phys. Lett. A* **374**, 3576–3584 (2010).
- ³⁰C. Yilmaz and N. Kikuchi, "Analysis and design of passive low-pass filter-type vibration isolators considering stiffness and mass limitations," *J. Sound Vib.* **293**, 171–195 (2006).
- ³¹C. Liu, X. Jing, and F. Li, "Vibration isolation using a hybrid lever-type isolation system with an X-shape supporting structure," *Int. J. Mech. Sci.* **98**, 169–177 (2015).
- ³²C. Liu, X. Jing, and Z. Chen, "Band stop vibration suppression using a passive X-shape structured lever-type isolation system," *Mech. Syst. Signal Process.* **68–69**, 342–353 (2016).
- ³³N. M. Frandsen, O. R. Bilal, J. S. Jensen, and M. I. Hussein, "Inertial amplification of continuous structures: Large band gaps from small masses," *J. Appl. Phys.* **119**, 124902 (2016).
- ³⁴S. Taniker and C. Yilmaz, "Design, analysis and experimental investigation of three-dimensional structures with inertial amplification induced vibration stop bands," *Int. J. Solids Struct.* **72**, 88–97 (2015).
- ³⁵O. Yuksel and C. Yilmaz, "Realization of an ultrawide stop band in a 2-D elastic metamaterial with topologically optimized inertial amplification mechanisms," *Int. J. Solids Struct.* **203**, 138–150 (2020).
- ³⁶L. Cao, Y. Zhu, Y. Xu, S.-W. Fan, Z. Yang, and B. Assouar, "Elastic bound state in the continuum with perfect mode conversion," *J. Mech. Phys. Solids* **154**, 104502 (2021).
- ³⁷Y. Zeng, L. Cao, S. Wan, T. Guo, Y.-F. Wang, Q.-J. Du, B. Assouar, and Y.-S. Wang, "Seismic metamaterials: Generating low-frequency bandgaps induced by inertial amplification," *Int. J. Mech. Sci.* **221**, 107224 (2022).
- ³⁸J. Li and S. Li, "Generating ultra wide low-frequency gap for transverse wave isolation via inertial amplification effects," *Phys. Lett. A* **382**, 241–247 (2018).
- ³⁹J. Mei, G. Ma, M. Yang, Z. Yang, W. Wen, and P. Sheng, "Dark acoustic metamaterials as super absorbers for low-frequency sound," *Nat. Commun.* **3**, 756 (2012).
- ⁴⁰J. Mei, X. Zhang, and Y. Wu, "Ultrathin metasurface with high absorptance for waterborne sound," *J. Appl. Phys.* **123**, 091710 (2018).
- ⁴¹Y. Ding, Z. Liu, C. Qiu, and J. Shi, "Metamaterial with simultaneously negative bulk modulus and mass density," *Phys. Rev. Lett.* **99**, 093904 (2007).
- ⁴²Y. Wang, C. Zhang, W. Chen, Z. Li, M. V. Golub, and S. I. Fomenko, "Precise and target-oriented control of the low-frequency Lamb wave bandgaps," *J. Sound Vib.* **511**, 116367 (2021).
- ⁴³Y.-F. Wang, J.-W. Liang, A.-L. Chen, Y.-S. Wang, and V. Laude, "Wave propagation in one-dimensional fluid-saturated porous metamaterials," *Phys. Rev. B* **99**, 134304 (2019).
- ⁴⁴R. Yang, W. Zhu, and J. Li, "Realization of 'trapped rainbow' in 1D slab waveguide with surface dispersion engineering," *Opt. Express* **23**, 6326–6335 (2015).
- ⁴⁵R. Cai, Y. Jin, T. Rabczuk, X. Zhuang, and B. Djafari-Rouhani, "Propagation and attenuation of Rayleigh and pseudo surface waves in viscoelastic metamaterials," *J. Appl. Phys.* **129**, 124903 (2021).
- ⁴⁶B. Graczykowski, F. Alzina, J. Gomis-Bresco, and C. Sotomayor Torres, "Finite element analysis of true and pseudo surface acoustic waves in one-dimensional phononic crystals," *J. Appl. Phys.* **119**, 025308 (2016).